PCCP

Direct observation of the cyclic dimer in liquid acetic acid by probing the C=O vibration with ultrafast coherent Raman spectroscopy

Journal:	*Physical Chemistry Chemical Physics*
Manuscript ID:	CP-ART-04-2014-001740.R1
Article Type:	Paper
Date Submitted by the Author:	27-Jun-2014
Complete List of Authors:	Lütgens, Matthias; University of Rostock, Institute of Physics Friedriszik, Frank; University of Rostock, Institute of Physics Lochbrunner, Stefan; University of Rostock, Institute of Physics

SCHOLARONE™
Manuscripts

Physical Chemistry Chemical Physics
CREATED USING THE RSC LaTeX PCCP ARTICLE TEMPLATE – SEE www.rsc.org/electronicfiles FOR DETAILS
ARTICLE TYPE www. rsc.org/xxxxxx | XXXXXXXX

Direct observation of the cyclic dimer in liquid acetic acid by probing the C=O vibration with ultrafast coherent Raman spectroscopy†

Matthias Lütgens, Frank Friedriszik and Stefan Lochbrunner*

Received Xth XXXXXXXXXX 20XX, Accepted Xth XXXXXXXXX 20XX
First published on the web Xth XXXXXXXXXX 200X
DOI: 10.1039/b000000x

We present a comparison of spontaneous Raman and ultrafast coherent anti-Stokes Raman scattering (CARS) spectra of the C=O vibration of liquid acetic acid. The former technique cannot clearly reveal the number of contributions in the spectrum. However, the additional time and spectrally resolved CARS experiment supports strictly the existence of four modes, which proves the coexistence of more than one H-bonded configuration in liquid acetic acid. A comparably slowly dephasing mode which is obscured by a broad band in the linear Raman spectrum is assigned to the cyclic dimer and can be observed well cleared from all other contributions by ultrafast CARS.

1 Introduction

H-bonding plays a decisive role for the structure, function and dynamics of a wide range of molecular systems.[1,2] It causes molecular network formation in liquids like water or determines the configuration of numerous biomolecules, like DNA and proteins,[3,4] polymers[5] or other complex supermolecular structures, highly relevant for life and engineering of new materials. The H-bonds are classified as directed, attractive interactions with binding energies in a range of 0.2 to 40 kcal/mol, which are in general lower than those of covalent or ionic bondings.[2] These properties are the main reasons for the importance of H-bonds as structural and functional elements in chemical reactions and life processes.

Molecules like acetic acid (AA) provide H-bond donor and acceptor sites at the same time.[6] This leads to different possible structural associates with total energies lower than that of the monomers. Since the binding energies differ only little between some of the assumed geometries and constant breaking and formation of hydrogen bonds occurs in hydrogen bonding liquids,[7] the coexistience of several conformers is possible. Also the environment of H-bonded molecular complexes can have strong impact on the structural motifs.[8–10] Determination of structures is a challenge in H-bond networks like in AA and still under intense investigation due to the manifold of energetically similar conformers and the fast dynamics within the network.

Prominent approaches for resolving structural network properties are scattering experiments, like x-ray and neutron scattering from which pair distribution functions can be obtained,[11] or vibrational spectroscopy. The latter measures either the frequencies of intermolecular vibrations of the H-bonded constituents, which are low frequent due to the heavy masses, or the frequencies of local vibrations involving the H-bond donors or acceptors. If donor or acceptor atoms are part of a H-bond, the vibrational frequencies of their eigenmodes are disturbed and a red shift of the resonance frequencies results reflecting the strength of the H-bond.[8,12] If different kinds of molecular arrangements can be adopted, broad and overlapping bands appear in the vibrational spectrum. Therefore, the decomposition of a vibrational spectrum into contributions assigned to individual structural motifs is a challenge. To assign such bands the sample itself can be manipulated, e.g. by substitution of isotopes, but this might change the physical properties of the molecular system due to the isotope effect.[1,13] The same applies to chemical substitution of side groups to prevent the formation of certain species by chemical blocking, which was successfully shown for AA in the gas phase.[14] Another promising approach to elucidate structural information hidden in broad features of linear spectra is applying spectroscopic techniques based on nonlinear effects.[15–18] Here, we compare spontaneous Raman spectra of acetic acid with time and frequency resolved coherent anti-Stokes Raman scattering (CARS). The Raman spectrum reflects the time averaged vibrational response of the Raman active vibrations. In multiplex time resolved CARS experiments a pump and a Stokes pulse drive a coherent superposition of a vibrational ground and an excited state.[19] A narrowband time delayed probe pulse is scattered at this coherence and samples the time evolution of the coherence decay. Due to the transient mapping of the coherences a separation in time between narrow and broad transitions can be achieved.[20]

† Electronic Supplementary Information (ESI) available: See DOI: 10.1039/b000000x/

Institut für Physik, Universität Rostock, Universitätsplatz 3, 18051 Rostock, Germany. Fax: 0049 381-4986802; Tel: 0049 381-4986960; E-mail: stefan.lochbrunner@uni-rostock.de

AA exists as planar cyclic dimers with C_{2h} symmetry in the gas phase[21] as well as in dilute nonpolar organic solvents.[9] This dimer is stabilized through two equal strong H-bonds of the form O−H···O=C. From ab-initio calculation it is known, that this structure is the most stable dimer geometry.[22–25] However, the H-bond network and its motifs in pure liquid AA are more complex and still under intense investigation.[6,23,25–28] During the last decades several experimental and theoretical investigations were performed. They suggest a manifold of different conformational geometries to be present in the liquid phase.[23–25,29,30] For AA in a supersonic jet structured low frequency spectra were measured clearly resolving the dimer modes.[31] In the liquid phase the low frequency modes are broadened[32,33] and a clear assignment is hindered. Nielsen et al. discussed the spectral features considering only modes of the cyclic dimer structure,[33] Nakabayashi et al. argued that also other geometries can contribute to the spectra.[23] Heisler et al. analyzed the low frequency Raman modes with polarization resolved optical Kerr effect measurements and concluded that cyclic dimers are the major components in liquid AA.[6] Since all publications argue that in AA complexes H-bonds of the form O−H···O=C and C−H···O=C with at least one carbonyl oxygen serving as H-bond acceptor exist,[24] the C=O vibration is an additional suitable indicator for the investigation of possible structures (see Fig. 1). Nakabayashi et al. performed Raman measurements on the C=O vibrations and assigned the observed bands by comparison to optimized geometries obtained by Hartree-Fock calculations.[23] They propose three contributions, C=O vibrations in which the carbonyl oxygen is strongly, weakly, or not at all involved in H-bonding. They argued with the help of temperature depended Raman measurements that the most abundant geometry are chain structures, as they are also found in solid AA.[34,35] Note, that the real chain like structure in the liquid might be much more corrugated as indicated in Fig. 1. However, the dominant feature at 1665 cm^{-1} (band I in Fig. 2a) in the Raman spectrum originates from the inner, strongly hydrogen bonded C=O modes of the linear chain. The asymmetric shoulder (band II) in the blue wing of the dominant band is caused by weaker hydrogen bonded C=O modes in the chain segments, but might also contain contributions from noncyclic dimers.[30] The mode with the highest frequency (band III) is assigned to free AA molecules or AA segments at the end of a chain.[23,30] The modes in the chain or larger aggregates are probably delocalized over some CO groups and the assignment describes their main character. Other groups introduced an additional vibrational component for discussing the dominant feature of the linear Raman spectrum.[29,30] They propose that the dominant band consists of two overlapping contributions, one resulting from the cyclic dimer, one from linear chains.[30] The cyclic dimer exhibits only one Raman active C=O stretch vibration with A_g symmetry.[36,37] In addition

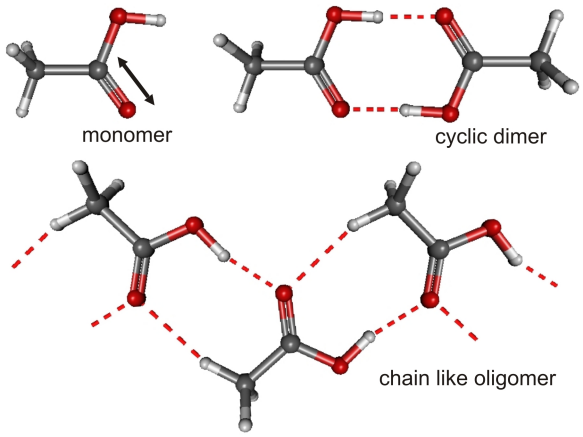

Fig. 1 Acetic acid structures: monomer, cyclic dimer and chain like structure. (black carbon, white hydrogen, red oxygen atoms)

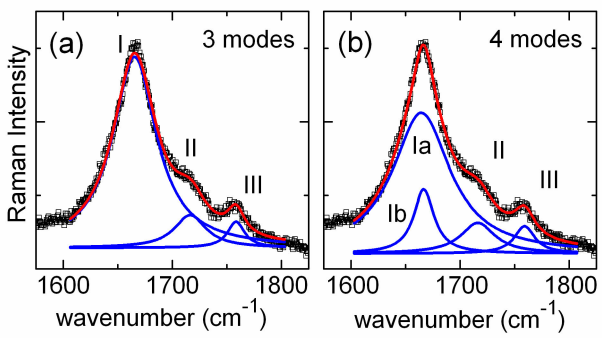

Fig. 2 Spontaneous Raman spectrum of AA (open circles) in the spectral region of the C=O vibration and fits (red lines) taking 3 (a, blue lines) and 4 modes (b, blue lines) into account.

to the Raman active mode, a pertinent, only IR active vibrational transition is known for this dimer. Génin et al. argued that the observed frequency splitting of the complimentary IR and Raman spectra is a strong hint for a geometry with inversion centre of the major species, that is the cyclic dimer.[27] Additionally, recent simulations of aggregated AA molecules showed that cyclic forms are preferred.[25] Motivated by this discussion on the interpretation of the signatures associated with the C=O vibration we perform multiplex CARS studies on AA. Here, we show that there is indeed a feature hidden beneath the dominant peak, which has to be assigned to the cyclic dimer.

2 Experimental setup and signal analysis

Spontaneous Raman spectra are measured in transmission using a combination of a laser diode with a laser line filter for excitation at 532 nm. Elastically scattered light is removed

This journal is © The Royal Society of Chemistry [year]

by a long pass Raman filter. The scattered Stokes signal is frequency resolved by an imaging spectrograph with a focal length of 300 mm equipped with an 1800 l/mm grating. The spectra are recorded with a CCD array detector. The spectral resolution of the setup is better than 8 cm^{-1}.

Time and frequency resolved CARS measurements are performed making use of ultrashort excitation of vibrational coherences and narrowband probing. Details of the setup are reported in the study of Lütgens *et al.* [38] and only a brief description is given here. The applied laser fields are generated by noncollinear optical parametric amplifiers (NOPAs) [39] pumped by a regenerative Ti:sapphire amplifier system (Spectra Physics, Spitfire Pro). A femtosecond NOPA with a subsequent prism compressor provides sub−50 fs Stokes pulses at 570 nm. A narrowband NOPA is used for the generation of pump and probe pulses with a bandwidth of 22 cm^{-1} at a center wavelength of approx. 510 nm. The pulses are generated via a conventionally NOPA followed by a bandpass filter and a noncollinear stage for amplification, pumped by the stretched second harmonic of the Ti:sapphire output. Pump, probe and Stokes pulses are focused into the sample fulfilling the phase matching condition by a BOXCARS arrangement. The CARS signal is spectrally resolved recorded with a spectrograph equipped with an array CCD detector. AA (Sigma Aldrich, purity 99.7%) samples are measured in a 2 mm thick fused silica cuvette placed in the beam focus.

The time dependent Raman response of a vibrational mode is modeled as a damped oscillator $R(t) = A_r \exp(-i\omega_{vib}t - \Gamma t)$ with an amplitude A_r, a resonance frequency ω_{vib}, and a damping constant Γ.[40] The spontaneous Raman signal results from the imaginary part of the Fourier transform of the response function [41] and exhibits a Lorentz profile. The damping constant Γ can be calculated from the full width $\Delta\tilde{\nu}$ at half maximum of the Raman band via $\Delta\tilde{\nu} = \Gamma/c\pi$. In the CARS experiment a coherent vibrational excitation is induced by the pair of pump and Stokes pulse and then sampled by the probe field. The resulting polarization causing the CARS signal can be expressed by the convolution of the Raman response function with the probe field and reads: [20,42]

$$\begin{aligned}\tilde{P}(\omega,t_D) &\propto n\int_0^\infty dt \exp[-i(\omega_{vib}-\omega)t-\Gamma t]E_{pr}(t_D,t)\\ &= iA^*\exp[-(\Gamma+i\Delta\omega)t_D]\exp\left[\frac{(\Gamma+i\Delta\omega)^2}{4\kappa_{pr}}\right]\\ &\times\left\{1+\mathrm{erf}\left[\frac{-i\Delta\omega+2\kappa_{pr}t_D-\Gamma}{2\sqrt{\kappa_{pr}}}\right]\right\} \quad (1)\end{aligned}$$

with $\Delta\omega = \omega_{vib} + \omega_{pr} - \omega$. During the pulse overlap two additional contributions appear in the signal field: (i) an additional polarization induced by the reverse time ordered fields $\tilde{P}_{pr\leftrightarrow pu}(\omega,t_D)$ and (ii) an instantaneous nonresonant contributuion due to the electronic response on the interacting fields $\tilde{P}_{NR}(\omega,t_D)$. The CARS intensity spectrum resulting from several vibrational contributions can be calculated from the squared absolute sum of the contributing polarizations:

$$\begin{aligned}\tilde{I}_{as}(t_D,\omega) &= \Big|\tilde{P}_{NR}(t_D,\omega)+\sum_i\left[\tilde{P}_i(t_D,\omega)\right.\\ &\left.+\tilde{P}_{pr\leftrightarrow pu,i}(t_D,\omega)\right]\Big|^2\mathrm{sinc}^2(\Delta kL/2) \quad (2)\end{aligned}$$

Here, the sinc function accounts for wavelength dependent phase matching for a sample length L. At early delay times the frequency resolved CARS signal is dominated by interferences between nonresonant and resonant contributions. After the cross-correlation only resonant contributions remain. In the applied homogeneous limit the spectral width of a resonance is given solely by the spectrum of the probe pulse, and its intensity decays mono exponentially with a time constant $T = 1/2\Gamma = T_2/2$. If fast dephasing modes causing broad peaks in the spontaneous Raman spectrum exist together with transitions with considerably slower dephasing times, a natural separation between these transitions can be observed in time resolved CARS measurements. While the fast dephasing modes fade quickly away the slower ones result in relatively strong signals also at later delay times. This will be important in the further discussion.

3 Results and discussion

3.1 Neat acetic acid

A typical linear Raman spectrum of AA in the spectral region of the C=O vibration is shown in Fig. 2. Clearly three contributions can be distinguished. The most intense peak is observed at approx. 1665 cm^{-1} (band I), a second contribution (band II) showing up as a shoulder of the dominant feature, and a third, well separated band (band III) at 1759 cm^{-1}. Following the arguments of Nakabayashi *et al.* [23] the spectrum can be decomposed into three Lorentzians as shown in Fig. 2a. The corresponding fit parameters are summarized in the first columns of Table I. Small deviations between fit and data arise close to the maximum of the main feature, but in general good agreement is achieved and the assumption of three contributions seems to be enough to reproduce the data. Since Lorentzians account only for pure homogenous dephasing, a better fit with more complex lineshapes can be expected. The discussed small deviation can also be removed by including a fourth transition in the fit, as shown in Fig. 2b. D'Amico analyzed Raman spectra of AA applying the Kubo-Anderson model, and argued that the main feature has to be decomposed into a narrow Lorentzian like contribution and a pronounced broad feature of more inhomogeneously broadened character. [30] Although we use only Lorentzians in the fit procedure, we find indications for a similar result; a combination of a

Table 1 Comparison of parameters extracted from fitting the linear Raman spectrum of liquid AA with 3 and 4 Lorentzians, respectively

	Spon. Raman: 3 modes			Spon. Raman: 4 modes	
No.	ω_{vib}/cm^{-1}	$\delta\omega_{vib}/cm^{-1}$	No.	ω_{vib}/cm^{-1}	$\delta\omega_{vib}/cm^{-1}$
I	1665	49	Ia	1665	64
			Ib	1667	23
II	1717	35	II	1716	38
III	1759	19	III	1759	23

narrow feature overlapped with a broad band leads to perfect agreement between fit and data.

From the spontaneous Raman spectrum it is hard to decide if only the three clearly seen modes are significant or if other relevant contributions are hidden beneath the dominant features. The interpretation of Raman spectra is often supported by the analysis of their polarization dependence and of isotope shifts. However, in the present case no additional insights are gained in this way. Polarized Raman spectra of AA and Raman spectra of deuterated derivatives are presented in the supporting information.† They provide no evidence, that a realistic decomposition of the spectrum calls for more than three vibrational contributions. To answer the question of the number of the involved vibrations we performed time and frequency resolved CARS measurements as they are shown in Fig. 3. The CARS signal exhibits the following characteristics. During the cross-correlation a defuse broad spectrum appears, which spectral contributions cannot be easily separated from each other. After the broad nonresonant signal vanishes, two contributions remain (Fig. 3a). These peaks are assigned to slowly dephasing, and therefore narrow resonances at $1668\,cm^{-1}$ and $1759\,cm^{-1}$. Frequency integrated time traces on a logarithmic scale show that these bands decay mono exponentially and can be described within the fast modulation limit (Fig. 3b). Dephasing times of $T_{2,I} = 0.43\,ps \pm 0.04\,ps$ and $T_{2,III} = 0.54\,ps \pm 0.05\,ps$ are found. The latter dephasing time fits to the line width of mode III measured by spontaneous Raman. However, $T_{2,I}$ corresponds to a line width of $25\,cm^{-1}$ which is in contradiction to the line width of $49\,cm^{-1}$ extracted from the Raman measurement assuming three modes. In between these contributions an additional spectral modulation appears in the CARS spectra, which vanishes with the nonresonant background. The spectral shape indicates that the contribution is not part of the nonresonant response, but has to be assigned to mode II appearing as shoulder in the spontaneous Raman spectrum.

To verify the number of included vibrational modes the complete CARS response was simulated. Before discussing these results we have to comment on the properties of the pulses used in the CARS experiment. Since the CARS signal is a convolution of the created vibrational coherence with the probe pulse, the probe characteristics are reflected in the

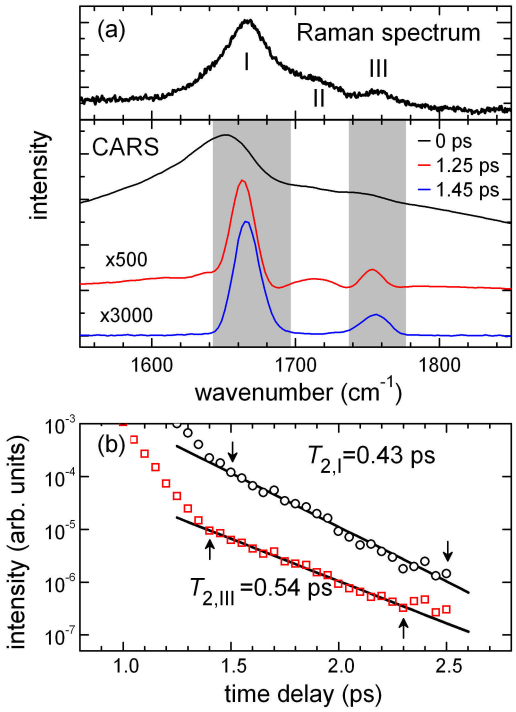

Fig. 3 (a) The Raman spectrum and time and frequency resolved CARS measurements of AA for the indicated time delays between probe and excitation pulses. Two features remain for longer times. The corresponding frequency integrated signals (intervals are highlighted in grey) and fitted exponential decays are shown in panel (b).

signal. Cross-correlation measurements have shown that the probe pulse is not Fourier limited. To account for the not ideal shape a pulse duration is chosen for the simulations, which is a compromise between the real pulse length and the Fourier limit of the probe spectrum. Therefore, some systematic deviations between the simulations and the CARS measurements are expected. Nevertheless, the fundamental features and spectral shapes should be reproduced. Especially, the CARS signal is very sensitive for slowly dephasing modes while time constants for the fast modes are hard to extract due to the restricted time resolution given by the picosecond probe pulse. A thorough discussion of the influence of the assumed pulse length on the results of the analysis is given in the supporting information.†

The following approach for the simulation is used: (i) Four resonant contributions are taken into account as suggested by Fig. 2 and 3, i.e. band I is constructed from two modes Ia and Ib. (ii) The dephasing times for the modes Ib and III are obtained from the decays of the frequency integrated CARS signals shown in Fig 3b. (iii) The fast dephasing contributions (band Ia and II) are included with dephasing times cal-

This journal is © The Royal Society of Chemistry [year]

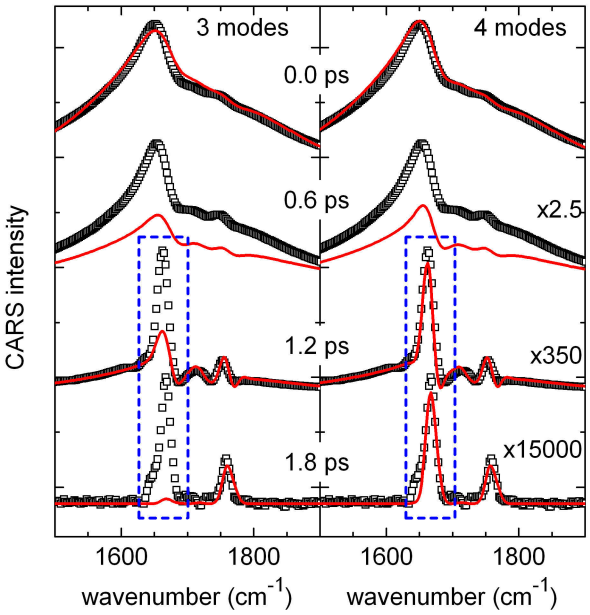

Fig. 4 Comparison between measured (open squares) and simulated (red lines) time and frequency resolved CARS spectra of the C=O modes in neat AA. On the left hand side 3 modes are taken into account while on the right hand side 4 modes are considered.

Table 2 Parameters used for simulating the CARS responses of neat acetic acid

	CARS: 3 modes			CARS: 4 modes	
No.	ω_{vib}/cm^{-1}	$\delta\omega_{vib}$/cm^{-1}	No.	ω_{vib}/cm^{-1}	$\delta\omega_{vib}$/cm^{-1}
I	1668	49	Ia	1669	53
			Ib	1668	25
II	1719	48	II	1719	48
III	1759	20	III	1759	20
$\delta_a CH_3$	1428	48	$\delta_a CH_3$	1428	48

culated from the line widths of the spontaneous Raman bands and slightly adopted to achieve best agreement with the CARS spectra. During the pulse overlap the vibrational resonances are contributing to the signal in a wide spectral range. Therefore, it is necessary to take the $\delta_a CH_3$ deformation mode at 1428 cm^{-1} into account (see also Fig. S3 in the supporting information[†]), since it contributes on the low frequency edge to the signal.[43] The center frequencies are only slightly varied compared to the values obtained from linear Raman as seen in Tab. 2. The resulting simulation is depicted in Fig. 4. For comparison we show also a simulation in which the slowly dephasing mode Ib is neglected and band I treated as a single resonance with a dephasing constant calculated from the Raman band.

Two regions with systematic deviations between measurements and simulations attract attention in Figure 4. The first

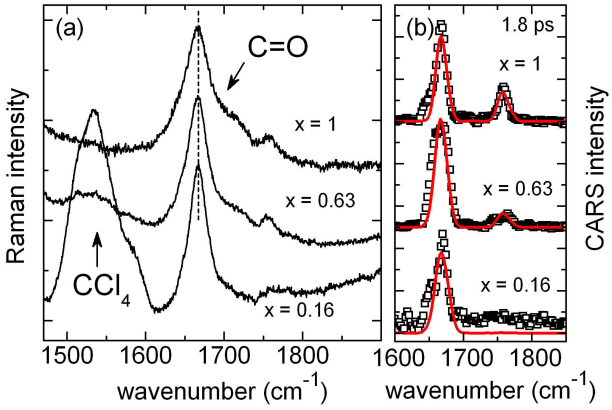

Fig. 5 (a) Raman spectra for different AA/CCl_4 ratios. x is the mole fraction of AA. (b) Scaled CARS spectra of the same samples after pulse overlap at a time delay of 1.8 ps. Squares represent measured data and red lines simulations.

deviation appears during pulse overlap because of the non Gaussian pulse shape of the probe pulses. But, although the intensity of the signal is underestimated, the signal modulation fits to the measured data at early delays. A simple intensity scaling of the measured data would lead also for a time delay of 0.6 ps to a satisfying agreement between simulation and measurement. The simulations for three and four contributions behave quite similar during the cross-correlation and in this time region it is difficult to pin down the number of relevant resonances.

The second deviation, marked by a blue box, only appears if we model the spectrum with three contributions and use dephasing constants taken from the linear Raman measurement. At late delay times a CARS signal at 1668 cm^{-1} remains while the simulation fades away. Using instead a contribution with a dephasing time of 0.43 ps obtained from the exponential fit good agreement after the cross-correlation can be achieved but the intensity and shape during the pulse overlap does not match to the measured signal. Only a combination of modes with a slow and a considerably fast dephasing time (mode Ia and Ib) reproduces the CARS signal as shown in the right panel of Fig. 4. From the combined analysis of the CARS and Raman spectra we have to conclude, that only the assumption of four contributions is in accordance with both measurements.

3.2 Acetic acid diluted in CCl_4

It is known that the cyclic AA dimer is the dominating molecular aggregate in very dilute solutions.[9] We use this finding to assign the contributions of the measured Raman and CARS spectra. Spontaneous Raman measurements on mixtures of AA and CCl_4 are shown in Figure 5a. The center frequency

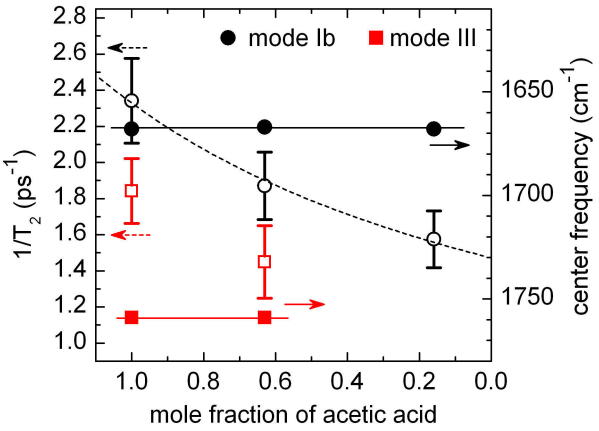

Fig. 6 Dephasing constants (open symbols) and center frequencies (solid symbols) in dependence of the concentration of AA in CCl_4 for the modes Ib (black symbols) and III (red symbols). The broken line visualizes the dependence of the dephasing times on the mole fraction of AA while the solid lines are horizontal demonstrating the constancy of the center frequencies. The dephasing rates are extracted from mono exponential fits of frequency integrated CARS signals.

of the main feature at 1665 cm^{-1} does not vary with increasing amount of solvent. But, the general shape of the spectra is changing reflecting the different structures found in the solutions. The dominant C=O band at 1665 cm^{-1} becomes narrower with decreasing AA concentration indicating that the narrowband resonance Ib gains relative weight and is the only remaining band at low AA concentrations. All other contributions lose intensity relative to this mode with decreasing AA content. The single remaining band corresponds to the molecular aggregate dominating at these conditions, i.e. the cyclic dimer. The mode is assigned to the C=O stretch vibration of this dimer.

Figure 5b shows concentration dependent CARS measurements on mixtures of AA and CCl_4 taken at a delay time of 1.8 ps after excitation. At that delay time two contributions are remaining in neat AA, bands Ib and III, and only one, band Ib, in the highly diluted sample. Concentration dependent spectra at various delay times are presented in the supporting information.[†] Figure 6 shows the vibrational frequencies and dephasing times of the modes Ib and III extracted from the CARS spectra. The fast dephasing contributions are not considered here due to the high uncertainty of the corresponding evaluation. The vibrational frequency of mode Ib, which is observed even at the lowest AA concentrations, does not vary with concentration supporting the notion that it belongs in all cases to the same and most stable aggregate. With this finding we can conclude that the narrow resonance Ib in neat AA is due to the cyclic dimer. The modes Ia, II and III are contributions from aggregates existing at higher AA concentrations, probably mostly linear chain aggregates as they are expected in the liquid.[23] The ab-initio calculations of Nakabayashi *et al.*[23] indicate that other structures are also possible and can contribute to mode II, too. The highest frequent contribution III is caused by C=O vibrations at the ends of the chain structure or by monomers, not embedded in the hydrogen bond network.

Dephasing is slowed down with increasing CCl_4 content for both analyzed modes Ib and III. The decreasing dephasing rate with an increasing number of CCl_4 molecules can be understood by correlating the dephasing time with collisions between molecules. To interpret the concentration dependent dephasing rate we assume the following simple equation for a binary mixture of AA molecules i with the mole fraction x and solvent molecules j:

$$2/T_2 = \rho(x)\left[k_{ii}x + k_{ij}(1-x)\right], \qquad (3)$$

similar to the model presented by Fickenscher *et al.*[44] Here, the rate k_{ii} describes collisions among AA aggregates and k_{ij} between AA and solvent molecules, which can be different. Resonant energy transfer between AA molecules might lead to an accelerated dephasing since it might reduce the lifetime of the monitored vibrational coherence. ρ is the number density accounting for the change of the particle density in the probe volume. The influence of concentration dependent radial distribution functions is neglected here. The molecular volume V_{CCl_4} of the solvent CCl_4 is by a factor $V_{CCl_4}/V_{AA} = 1.7$ larger than that of V_{AA}. The broken line in Figure 6 is obtained by applying Equ. 3 to the extracted dephasing parameters. The fit reveals a ratio of the collision rates of $k_{ii}/k_{ij} = 0.93$. If resonant energy transfer processes would strongly contribute, the rate k_{ii} for collisions between AA molecules should be larger than k_{ij}. Since this is not the case, dephasing is dominated by nonresonant nearest neighbor collisions and therefore mainly dependent on the particle density.

4 Conclusions

From the obtained results the following connections between the spectroscopic signatures and the structural properties of liquid AA are proposed. The liquid is a mixture of cyclic dimers and chain like structures. Other structures may be present to some extent, too. In accord with the studies of Nakabayashi *et al.*[23] and D'Amico *et al.*[30] the C=O modes of chains and other complexes are assigned to the broad peaks at 1665 cm^{-1} and 1716 cm^{-1}, which vanish in the CARS spectra quickly with time. The mode at 1759 cm^{-1} is not or only weakly affected by hydrogen bonding and originates from end segments of the chain structures or from monomers. Under the broad main feature of the spectrum (band I) a mode at

This journal is © The Royal Society of Chemistry [year]

$1668\,cm^{-1}$ is hidden which can be observed by time resolved CARS and which exhibits a comparably slow coherence decay. This contribution cannot be isolated by polarization dependent Raman measurements or by Raman spectra of deuterated AA derivates.[†] From its concentration dependent behavior we assign this mode to the C=O stretch vibration of the cyclic dimer. As the CARS measurements show dephasing of this mode is quite slow compared to C=O modes of other AA complexes. This can be understood in terms of the closed ring configuration which is stabilized by two strong H-bonds resulting in a rather rigid and well defined geometry compared to open structures. The concentration dependence of the dephasing time in binary mixtures with CCl_4 reflects the variation of the particle density and indicates that dephasing is mainly caused by nonresonant collisions.

Time resolved CARS allows to separate the mode of the cyclic dimer from contributions of other complexes in pure AA and to investigate its specific properties. Furthermore, the technique opens the possibility for direct investigation of a substructure in a mixture of complexes by pump-probe measurements.

Acknowledgement

The authors acknowledge financial support by the Deutsche Forschungsgemeinschaft through the collaborative research center SFB 652.

References

1 G. Jeffrey, *An Introduction to Hydrogen Bonding*, Oxford University Press, 1997.
2 T. Steiner, *Angew. Chem. Int. Ed.*, 2002, **41**, 48–76.
3 J. D. Watson and F. H. C. Crick, *Nature*, 1953, **171**, 737–738.
4 L. Pauling and R. B. Corey, *Proc. Natl. Acad. Sci.*, 1951, **37**, 235–240.
5 G. Armstrong and M. Buggy, *J. Mater. Sci.*, 2005, **40**, 547–559.
6 I. A. Heisler, K. Mazur, S. Yamaguchi, K. Tominaga and S. R. Meech, *Phys. Chem. Chem. Phys.*, 2011, **13**, 15573–15579.
7 J. B. Asbury, T. Steinel, C. Stromberg, K. J. Gaffney, I. R. Piletic and M. D. Fayer, *J. Chem. Phys.*, 2003, **119**, 12981–12997.
8 A. Allerhand and P. von R. Schleyer, *J. Am. Chem. Soc.*, 1963, **85**, 371–380.
9 Y. Fujii, H. Yamada and M. Mizuta, *J. Phys. Chem.*, 1988, **92**, 6768–6772.
10 T. Nakabayashi, H. Sato, F. Hirata and N. Nishi, *J. Phys. Chem. A*, 2001, **105**, 245–250.
11 V. Petkov, in *Pair Distribution Functions Analysis*, John Wiley&Sons, Inc., 2002.
12 S. Grabowski, *Hydrogen Bonding - New Insights*, Springer, 2006.
13 A. Kohen and H. Limbach, *Isotope Effects In Chemistry and Biology*, Taylor & Francis, 2005, pp. 281–304.
14 C. Emmeluth and M. A. Suhm, *Phys. Chem. Chem. Phys.*, 2003, **5**, 3094–3099.
15 W. Zinth, M. Nuss and W. Kaiser, *Opt. Commun.*, 1983, **44**, 262 – 266.
16 I. Noda, *J. Am. Chem. Soc.*, 1989, **111**, 8116–8118.
17 P. Hamm, M. Lim and R. M. Hochstrasser, *J. Phys. Chem. B*, 1998, **102**, 6123–6138.
18 W. Zhao and J. C. Wright, *J. Am. Chem. Soc.*, 1999, **121**, 10994–10998.
19 T. Chen, A. Vierheilig, W. Kiefer and A. Materny, *Phys. Chem. Chem. Phys.*, 2001, **3**, 5408–5415.
20 M. Lütgens, S. Chatzipapadopoulos, F. Friedriszik and S. Lochbrunner, *J. Raman Spectrosc.*, 2014, **45**, 359–368.
21 J. Derissen, *J. Mol. Struct.*, 1971, **7**, 67 – 80.
22 L. Turi and J. J. Dannenberg, *J. Phys. Chem.*, 1993, **97**, 12197–12204.
23 T. Nakabayashi, K. Kosugi and N. Nishi, *J. Phys. Chem. A*, 1999, **103**, 8595–8603.
24 J. Chocholoušová, J. Vacek and P. Hobza, *J. Phys. Chem. A*, 2003, **107**, 3086–3092.
25 W. Xu and J. Yang, *J. Phys. Chem. A*, 2010, **114**, 5377–5388.
26 A. Burneau, F. Génin and F. Quilès, *Phys. Chem. Chem. Phys.*, 2000, **2**, 5020–5029.
27 F. Génin, F. Quilès and A. Burneau, *Phys. Chem. Chem. Phys.*, 2001, **3**, 932–942.
28 N. B. Zineb, A. Chebaane, F. Hammami, M. Bahri and S. Nasr, *J. Mol. Liq.*, 2012, **173**, 164 – 171.
29 J. B. Ng, B. Petelenz and H. F. Shurvell, *Can. J. Chem.*, 1988, **66**, 1912–1918.
30 F. D'Amico, F. Bencivenga, A. Gessini, E. Principi, R. Cucini and C. Masciovecchio, *J. Phys. Chem. B*, 2012, **116**, 13219–13227.
31 Z. Xue and M. A. Suhm, *Mol. Phys.*, 2010, **108**, 2279–2288.
32 P. Waldstein and L. A. Blatz, *The Journal of Physical Chemistry*, 1967, **71**, 2271–2276.
33 O. F. Nielsen and P. Lund, *J. Chem. Phys.*, 1983, **78**, 652–655.
34 R. E. Jones and D. H. Templeton, *Acta Crystallogr.*, 1958, **11**, 484–487.
35 P.-G. Jönsson, *Acta Crystallogr.*, 1971, **B27**, 893–898.
36 J. E. Bertie and K. H. Michaelian, *J. Chem. Phys.*, 1982, **77**, 5267–5271.
37 J. Dreyer, *J. Chem. Phys.*, 2005, **122**, 184306.
38 M. Lütgens, S. Chatzipapadopoulos and S. Lochbrunner, *Opt. Express*, 2012, **20**, 6478–6487.
39 E. Riedle, M. Beutter, S. Lochbrunner, J. Piel, S. Schenkl, S. Spörlein and W. Zinth, *Appl. Phys. B*, 2000, **71**, 457–465.
40 D. C. Urbanek and M. A. Berg, *J. Chem. Phys.*, 2007, **127**, 044306.
41 M. Cho, M. Du, N. F. Scherer, G. R. Fleming and S. Mukamel, *J. Chem. Phys.*, 1993, **99**, 2410–2428.
42 S. Nath, D. C. Urbanek, S. J. Kern and M. A. Berg, *J. Chem. Phys.*, 2007, **127**, 044307.
43 J. B. Ng and H. F. Shurvell, *J. Phys. Chem.*, 1987, **91**, 496–500.
44 M. Fickenscher, H.-G. Purucker and A. Laubereau, *Chem. Phys. Lett.*, 1992, **191**, 182 – 188.